The Astrophysical Journal, 755:122 (7pp), 2012 August 20 doi:10.1088/0004-637X/755/2/122

HOT AND COLD SPOT COUNTS AS PROBES OF NON-GAUSSIANITY IN THE COSMIC MICROWAVE BACKGROUND

Pravabati Chingangbam[1], Changbom Park[2], K. P. Yogendran[3], and Rien van de Weygaert[4]
[1] Indian Institute of Astrophysics, Koramangala II Block, Bangalore 560034, India; prava@iiap.res.in
[2] Korea Institute for Advanced Study, 85 Hoegiro, Dongdaemun-gu, Seoul 130-722, Republic of Korea; cbp@kias.re.kr
[3] Indian Institute for Science Education and Research, Mohali, India; pattag@gmail.com
[4] Kapteyn Astronomical Institute, University of Groningen, P.O. Box 800, 9747 AV Groningen, The Netherlands; weygaert@astro.rug.nl
Received 2012 April 23; accepted 2012 May 31; published 2012 August 2

ABSTRACT

We introduce the numbers of hot and cold spots, n_h and n_c, of excursion sets of the cosmic microwave background (CMB) temperature anisotropy maps as statistical observables that can discriminate different non-Gaussian models. We numerically compute them from simulations of non-Gaussian CMB temperature fluctuation maps. The first kind of non-Gaussian model we study is the local type primordial non-Gaussianity. The second kind of model has some specific form of the probability distribution function from which the temperature fluctuation value at each pixel is drawn, obtained using HEALPIX. We find the characteristic non-Gaussian deviation shapes of n_h and n_c, which is distinct for each of the models under consideration. We further demonstrate that n_h and n_c carry additional information compared to the genus, which is just their linear combination, making them valuable additions to the Minkowski Functionals in constraining non-Gaussianity.

Key words: cosmic background radiation – early universe

Online-only material: color figures

1. INTRODUCTION

The statistical nature of the cosmic microwave background (CMB) radiation temperature fluctuation field that we see today must be predominantly inherited from those of the primordial density fluctuations. Inflation is currently the forerunner among possible mechanisms that could have produced the primordial density perturbations. All models of inflation, in general, predict some amount of deviation of these fluctuations from a Gaussian distribution, with the details of the deviations being model dependent. The knowledge of these deviations, if observed, for example, in the CMB, will thus be of much value in distinguishing among various models of inflation. The observational search for primordial non-Gaussianity, however, is not easy since various observational effects can mask the true CMB signal. Given this difficulty the need for efficient, sensitive, and complementary observables that can characterize non-Gaussian deviations cannot be overemphasized.

Popular statistical measures of non-Gaussianity that can be obtained from the CMB fall under two broad categories. The first are observables that are defined in harmonic space (Komatsu et al. 2011; Smidt et al. 2010; Curto et al. 2011; Vielva & Sanz 2010) such as the bispectrum, trispectrum, wavelets, the spherical Mexican hat wavelet, etc. The second category consists of those that directly exploit the geometric and topological properties of the temperature fluctuation field. A popular class of observables, the Minkowski Functionals (MFs; Tomita 1986; Coles 1988; Gott et al. 1990; Schmalzing & Gorski 1998; Winitzki & Kosowsky 1998), has long been applied to constrain non-Gaussianity in the CMB. Considerable progress has been made in understanding them analytically for weakly non-Gaussian random fields (Matsubara 2003; Hikage et al. 2006, 2008; Komatsu et al. 2009; Pogosyan et al. 2009; Matsubara 2010; Gay et al. 2012). Of the three MFs that can be defined for a two-dimensional random field, the third one, known as the genus, is a topological quantity which depends on the global properties of the random field. It is given by the difference of the numbers of hot and cold spots at any given temperature fluctuation field value. The genus and other MFs have non-Gaussian deviation shapes that are characteristic of the non-Gaussian model. The non-Gaussian deviation shape of each observable tells us what field values are best probed by the observable, and these are the values where the deviations are the largest.

In this paper, we introduce the numbers of hot and cold spots as statistical observables in their own right. Just like the genus, they are topological quantities that depend only on the global properties of the temperature fluctuation field. They have been studied earlier by Coles and Barrow (Coles & Barrow 1987) and an approximate formula is known for Gaussian and some non-Gaussian random fields (Vanmarcke 1983). Our goal here is to determine their sensitivity and non-Gaussian deviation shapes as signatures of various kinds of non-Gaussianities. We have computed them using numerical methods from simulated non-Gaussian CMB maps. We first compute them for simulations containing the so-called local type primordial non-Gaussian model parameterized by $f_{\rm NL}$ (Liguori et al. 2003) and $g_{\rm NL}$ (Chingangbam & Park 2009). We also compute them using non-Gaussian simulations provided by HEALPIX (Rocha et al. 2005; Górski et al. 2005). We have obtained the characteristic non-Gaussian deviations for these different types of input primordial non-Gaussianity.

We do not intend to address all the issues of observational systematic effects in this first paper but instead focus on the theoretical understanding of their behavior upon potential non-Gaussianity. The expectation in introducing them is that we can get additional information about non-Gaussian fields by using these two observables in addition to the genus and other MFs. Since the genus is given by the difference between these two numbers, in taking their linear combination we are throwing away some information. This expectation will be most justified if the number of hot spots is independent of the number of

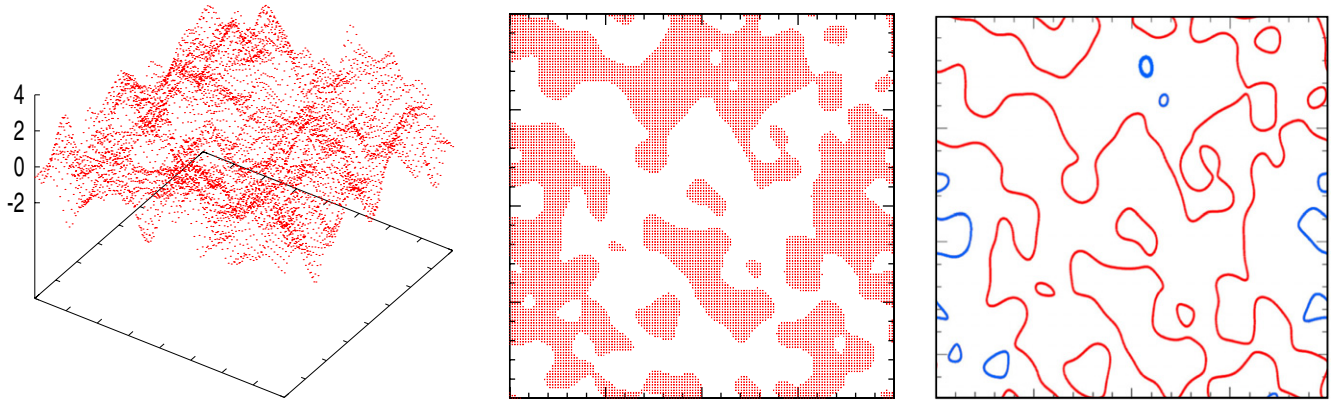

Figure 1. Left panel: a patch of a smoothed Gaussian fluctuation field. The field is defined on a square with periodic boundary condition so field values that are at opposite ends of the square are identified. The y-axis gives the level value, ν. Middle panel: the red regions give the excursion set for $\nu = 0$. The set is fragmented into several contiguous or connected regions. Some of the connected regions have holes within them. Each connected region is called a hot spot while each hole is called a cold spot. Right panel: iso-temperature contours enclosing the excursion region (red lines) and holes (blue lines) for $\nu = 0$. One can see partial contours that are located at extreme ends of the square which together form closed contours. n_h is the number of isolated connected regions, which can be obtained by counting the closed red contours. n_c is the number of holes within the connected regions and can be obtained by counting the blue contours.

(A color version of this figure is available in the online journal.)

cold spots. As we will see in Section 3, this is not always the case and whether they are independent or not depends on the non-Gaussian model. For example, for the local type primordial non-Gaussian model parameterized by $f_{\rm NL}$ and $g_{\rm NL}$, we find that they are related to each other in a specific way. However, even for the models where they are related, there is still the additional gain of information coming from the fact that they have non-Gaussian deviation shapes that are quite distinct from those of the genus and the other MFs and hence they best extract non-Gaussian deviations of the field at values different from the MFs. Therefore, they carry information that is complementary to the MFs. We further calculate the uncertainties in the numbers of hot and cold spots, taking into account cosmic variance, instrumental noise, and sample boundaries at our choice of smoothing scales. We demonstrate that there exists additional information in the numbers of hot and cold spots compared to the genus, as shown in Section 4.

This paper is organized as follows: in Section 2, we briefly describe excursion sets and hot and cold spots, followed by our method for numerically computing them. We then show the results for the numbers of hot and cold spots computed from Gaussian CMB temperature fluctuation maps. In Section 3, we present the non-Gaussian deviations of the numbers of hot and cold spots for the different kinds of non-Gaussianity that we have studied, first, the local type non-Gaussianity and second for the input non-Gaussian probability distribution function (PDF) models obtained using HEALPIX. In Section 4, we analyze how observational effects such as beam profiles, instrument noise, and incomplete sky coverage affect the numbers of hot and cold spots by computing them from simulations to which these effects have been added. Further, we compare their sensitivity to non-Gaussianity with that of the genus and show that they can give more information than the genus. We end with a summary and discussion of the implications of our results in Section 5.

2. HOT AND COLD SPOT COUNTS

Let $f \equiv (T(\hat{n}) - T_0)/T_0$ denote the CMB temperature anisotropy field, where T_0 denotes the mean temperature. By rescaling f by its rms value, σ_0, we can define the *threshold temperature*, $\nu \equiv f/\sigma_0$. At each value of ν, if we consider the set of all pixels that have values equal to or above ν we obtain what is usually referred to as an *excursion set*. This set consists of many *connected regions* into which the temperature field "manifold" has fractured, and *holes* within those regions due to the excluded pixels. As is commonly done in the literature, we call each connected region a *hot spot* and each hole a *cold spot*. For an excursion set indexed by ν, we define

1. $n_h \equiv$ number of hot spots and
2. $n_c \equiv$ number of cold spots.

As we change ν, the excursion sets behave as though they are a one-parameter family of spaces parameterized by ν, and their properties such as the numbers of the hot and cold spots change systematically as a function of ν.

We can relate the numbers of hot and cold spots to the numbers of closed iso-temperature contours. The boundaries of each excursion set are iso-temperature contours for the corresponding ν. We can assign an orientation to each of the contours—positive for those that enclose hot spots and negative for the ones that enclose cold spots. n_h and n_c are then simply counts of closed positive and negative orientation contours, respectively. For the purpose of illustration, in Figure 1 we have shown a smoothed Gaussian random field defined on a square with periodic boundary condition. The left panel shows the full field. The middle panel shows the excursion set for the same field for $\nu = 0$. Connected regions and holes are clearly visible. The right panel shows the boundary or iso-temperature contours for the same excursion set—red enclosing hot spots and blue enclosing cold spots.

Mathematically, we can express n_h and n_c as line integrals

$$n_h = \frac{1}{2\pi}\int_{C_+} K\, ds, \quad n_c = \frac{1}{2\pi}\int_{C_-} K\, ds, \tag{1}$$

where K is the total curvature of iso-temperature contours for each ν. C_+ denotes contours that enclose hot spots while C_- denotes contours that enclose cold spots. The genus, g, is given by a linear combination of n_h and n_c:

$$g(\nu) = n_h(\nu) - n_c(\nu). \tag{2}$$

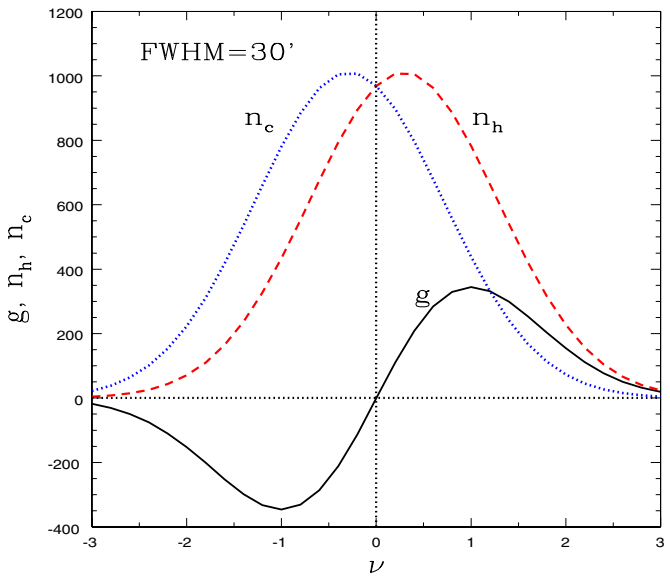

Figure 2. n_h, n_c, and g measured from Gaussian simulations smoothed with FWHM=30′. The y-axis values are per unit area of the sphere. The plots are average over 200 simulations.

(A color version of this figure is available in the online journal.)

For a Gaussian fluctuation field, g is given by the expression

$$g(\nu) = A\,\nu\,e^{-\nu^2/2}, \tag{3}$$

where the amplitude A carries the physical information about the field and is given by $A = (1/2\pi^3)(\sigma_1/\sigma_0)^2$, with σ_1 being the rms of the gradient field.

Note that we could equivalently define our excursion set at each ν to consist of the pixels having values below ν, in which case the definitions of n_h and n_c would get interchanged.

2.1. Numerical Method for Computing the Numbers of Hot and Cold Spots

Our method for computing the numbers of hot and cold spots is based on the method for computing the genus outlined in Gott et al. (1990). It is essentially an implementation of Equation (1) based on connecting iso-temperature pixels with the information of the orientation of the contour retained. At the end contours with the same orientation are counted to get n_h and n_c.

In Figure 2, we have shown n_h, n_c, and g versus ν obtained by averaging over measurements from 200 simulated Gaussian CMB anisotropy maps with the HEALPIX resolution parameter $Nside = 512$ and smoothed with a Gaussian filter with FWHM= 30′. The simulations have ΛCDM parameter values given by WMAP 5 year data (Komatsu et al. 2009). The Gaussian genus formula serves to test the accuracy of the numerical computation of n_h and n_c (unless of course there is some error which contributes equally to both n_h and n_c and cancels out for the genus). It has been shown in C. Park et al. (2012, in preparation) that precise details of the numbers of hot and cold spots in terms of Betti numbers for Gaussian random fields such as the amplitude and location of peaks vary significantly as we vary the power index, n, of the input three-dimensional power spectrum $P(k) \propto k^{-n}$. The trend is that as n increases the amplitude increases and the peak shifts closer to $\nu = 0$. For $n \sim 3$, which is relevant for the CMB, the result that we have obtained is in agreement with this trend.

3. NON-GAUSSIAN DEVIATIONS OF THE NUMBERS OF HOT AND COLD SPOTS

In this section, we compute the non-Gaussian deviations of numbers of hot and cold spots for different models of primordial non-Gaussianity.

3.1. Local Type Primordial Non-Gaussianity

We consider the following expansion to cubic order of the primordial gravitational potential:

$$\Phi(\boldsymbol{x}) = \Phi^G(\boldsymbol{x}) + f_{\rm NL}((\Phi^G(\boldsymbol{x}))^2 - \langle(\Phi^G)^2\rangle) + g_{\rm NL}(\Phi^G(\boldsymbol{x}))^3 + \cdots, \tag{4}$$

where Φ^G is a Gaussian potential and $f_{\rm NL}$ and $g_{\rm NL}$ are constants which parameterize the first and second order nonlinearities, respectively, in the gravitational potential. Then, expanding the CMB temperature fluctuation field in multipoles, as $f = \sum_{\ell m} a_{\ell m} Y_{\ell m}$, we can calculate $a_{\ell m}$ by convolving Φ with the full radiation transfer function Δ_ℓ, as

$$a_{\ell m} = 4\pi(-i)^\ell \int \frac{d^3k}{(2\pi)^3}\,\Phi(\boldsymbol{k}, t_i)\,\Delta_\ell(k, t_0)\,Y^*_{\ell m}(\hat{k}). \tag{5}$$

We use simulations of non-Gaussian CMB maps (Liguori et al. 2003; Chingangbam & Park 2009) which have Equation (4) as the input potential to calculate $a_{\ell m}$. The input power spectrum of Φ^G is given as $P_\Phi(k) = (A_0/k^3)(k/k_0)^{n_s-1}$, where A, n_s, and k_0 are taken from WMAP 5 year ΛCDM parameter values (Komatsu et al. 2009). The simulation resolution used is given by $Nside = 512$, as in Section 2.1. We use Δ_ℓ calculated with all perturbation terms kept to linear order (Seljak & Zaldarriaga 1996) and hence the non-Gaussianity that shows up in the resulting CMB temperature field is a direct consequence of the primordial input. We have computed n_h and n_c for three kinds of simulations—pure $f_{\rm NL}$, pure $g_{\rm NL}$, and a mixture of the two. In order to quantify the non-Gaussian deviations we define

$$\Delta n_i = n_i^{\rm NG} - n_i^G, \tag{6}$$

where i stands for h or c, the index G stands for Gaussian, and NG for non-Gaussian. Plots are shown normalized by $n_i^{G,\max}$, which is the amplitude of n_i^G.

In Figure 3, we have plotted Δn_h and Δn_c versus ν for pure $f_{\rm NL}$ and pure $g_{\rm NL}$ cases. We have used the values $f_{\rm NL} = \pm 100$ and $g_{\rm NL} = \pm 1 \times 10^6$ and shown plots for two smoothing angles—FWHM = 30′ and 90′. For each case, it is important to note that Δn_i has a characteristic non-Gaussian deviation shape and they can be easily distinguished from each other. There is slight variation of the deviation shapes as functions of the smoothing angle. Roughly speaking, the magnitude of the deviation at higher threshold values $|\nu| \gtrsim 2$ is larger for larger smoothing angles. An interesting observation is that for each case we can see that n_h and n_c are correlated as

$$\begin{aligned} \Delta n_h(\nu, f_{\rm NL}) &= -\Delta n_c(-\nu, f_{\rm NL}) \\ \Delta n_h(\nu, g_{\rm NL}) &= \Delta n_c(-\nu, g_{\rm NL}). \end{aligned} \tag{7}$$

In Figure 4 we have plotted Δn_h versus Δn_c at each value of ν for pure $f_{\rm NL}$ (green, solid line) and for pure $g_{\rm NL}$ (brown, dotted) models. This is another way of visualizing the characteristics of the non-Gaussianity caused by $f_{\rm NL}$ or $g_{\rm NL}$. Figure 5 shows Δn_i for the case when both $f_{\rm NL}$ and $g_{\rm NL}$ contribute to the primordial non-Gaussianity for the same smoothing angles and parameter values. If we compare with non-Gaussian deviations of the genus

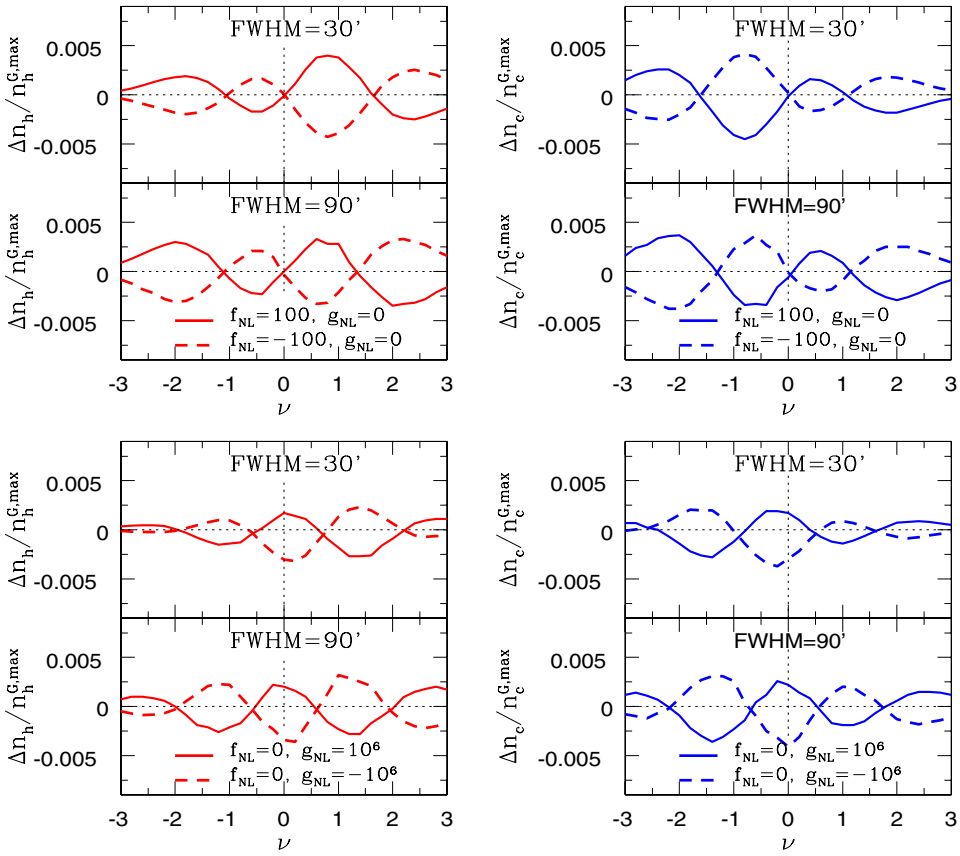

Figure 3. Non-Gaussian deviations of n_h and n_c for pure $f_{\rm NL}$ (upper panels) and pure $g_{\rm NL}$ (lower panels) input primordial non-Gaussianity at two smoothing angles—FWHM = 30′ and 90′. Δn_i is defined as given in Equation (6). $n_i^{G,\rm max}$ is the maximum value of $n_i^G(\nu)$. The y-axis values are per unit area of the sphere. The simulations have WMAP 5 year ΛCDM parameter values. The results are average over 200 simulations.

(A color version of this figure is available in the online journal.)

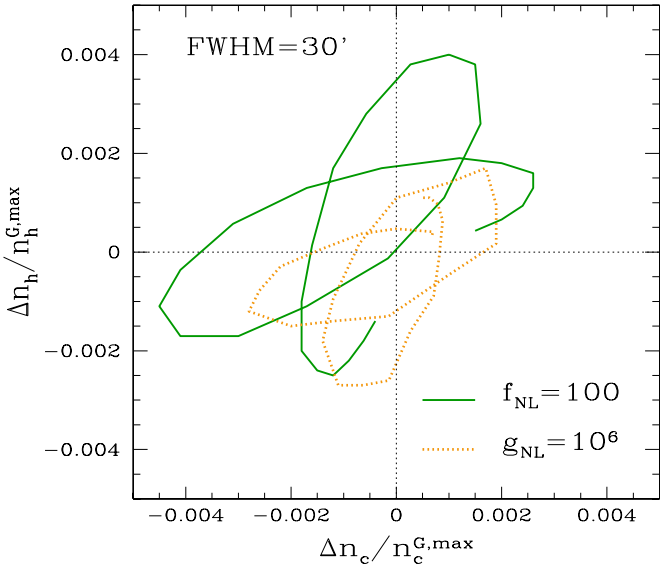

Figure 4. Plots of Δn_h vs. Δn_c for pure $f_{\rm NL}$ (green, solid line) and for pure $g_{\rm NL}$ (brown, dotted) models. This is a different way of showing the characteristics of the non-Gaussianity caused by the $f_{\rm NL}$ and $g_{\rm NL}$ terms.

(A color version of this figure is available in the online journal.)

(see Figure 2 of Hikage et al. 2006 for pure $f_{\rm NL}$ case and Figure 4 of Chingangbam & Park 2009 for pure $g_{\rm NL}$ case), we find that the amplitude of the deviations of n_h and n_c are smaller by about a factor of two.

We can get some idea about the dependence of Δn_h and Δn_c on $f_{\rm NL}$ and $g_{\rm NL}$ from the analytic expressions of the non-Gaussian deviation of the genus (Hikage et al. 2006; Matsubara 2003), which is given as an expansion in powers of σ_0. For pure $f_{\rm NL}$ and pure $g_{\rm NL}$ cases, keeping the genus expansion up to σ_0 and σ_0^2 orders, respectively, the genus non-Gaussian deviations have linear dependence on $f_{\rm NL}$ and $g_{\rm NL}$. When both $f_{\rm NL}$ and $g_{\rm NL}$ are present, then at σ_0^2 order there must be cross terms containing both $f_{\rm NL}$ and $g_{\rm NL}$. Hence the non-Gaussian deviation of the genus will not be a simple linear combination of deviation terms depending on $f_{\rm NL}$ and $g_{\rm NL}$ independently. Since the genus is just the subtraction of n_c from n_h, we can expect n_c and n_h to behave in a roughly similar fashion.

3.2. HEALPIX Non-Gaussian Models

We have generated non-Gaussian maps using the HEALPIX routine sky_ng_sim (Rocha et al. 2005; Górski et al. 2005). This program implements two kinds of non-Gaussian models. The first is a model where the input probability distribution function is taken to be an expansion in excited states of the simple harmonic oscillator (SHO model), as given below:

$$P(f) = e^{-f^2/2\sigma_0^2}\left|\sum_{i=0}^{n}\alpha_i C_i H_i\left(\frac{f}{\sqrt{2}\sigma_0}\right)\right|^2, \qquad (8)$$

where H_i are Hermite polynomials, C_i are normalization constants, σ_0 is the variance of the Gaussian PDF, and α_i, for $i \geqslant 1$, are free parameters. α_0 is constrained to be $\alpha_0 = \sqrt{1-\sum_i^n |\alpha_i|^2}$. For

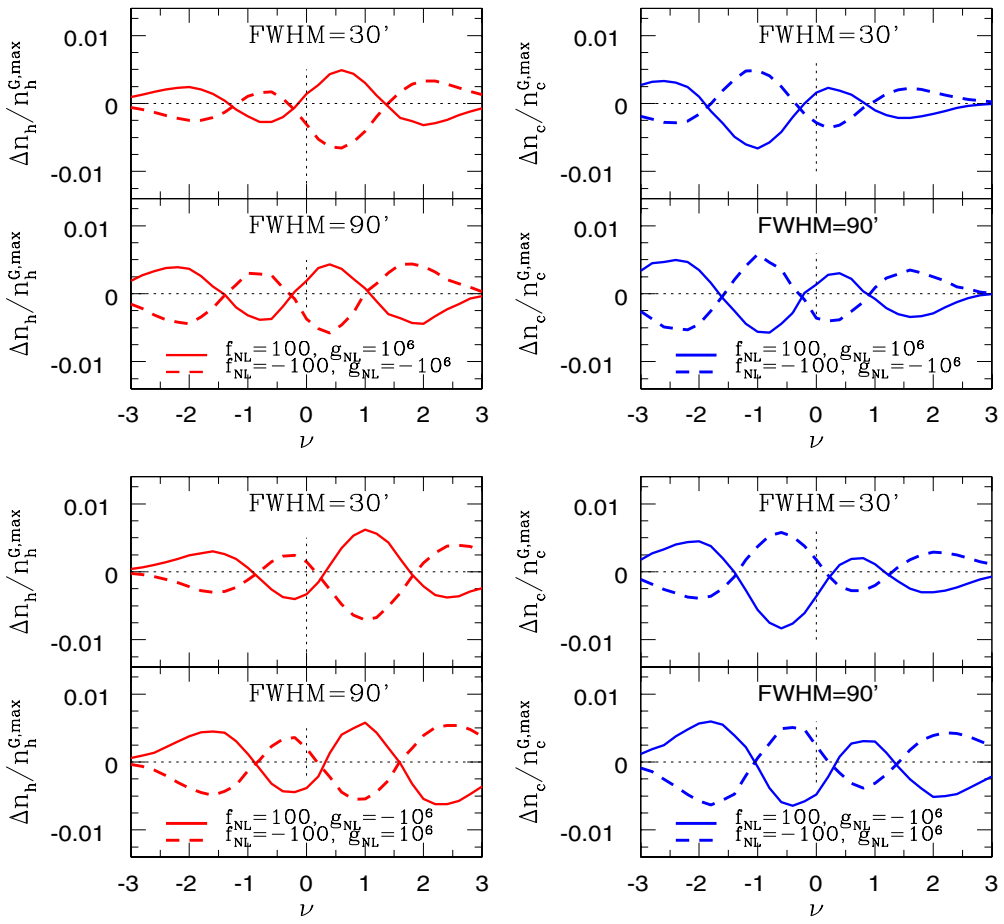

Figure 5. Same as in Figure 3 for a mixture of $f_{\rm NL}$ and $g_{\rm NL}$ input primordial non-Gaussianity.
(A color version of this figure is available in the online journal.)

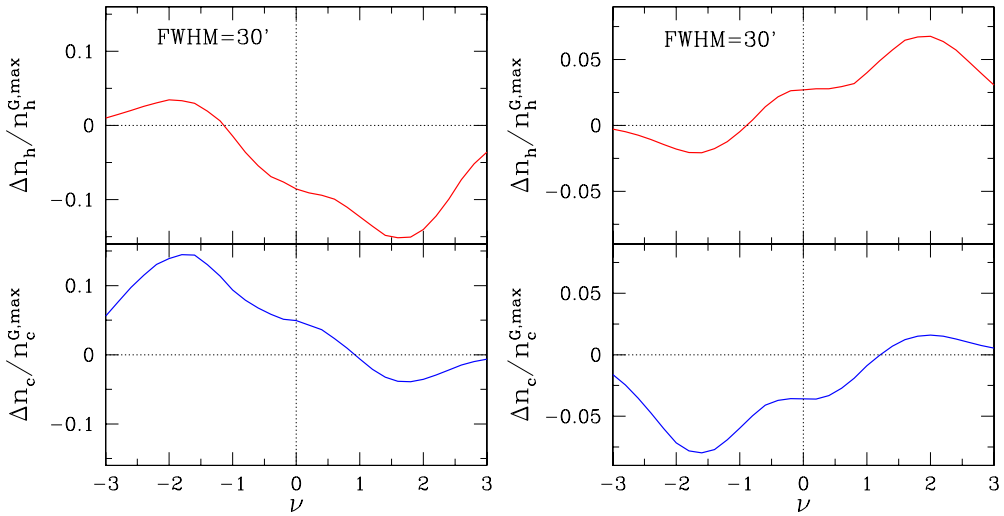

Figure 6. Left panel: Δn_i for the SH0 model. We have used $\alpha_1 = 0.6$ and $\alpha_2 = 0.6$. Right panel: Δn_i for Gaussian power model. We have used $p = 1$. The plots are average over 50 maps.
(A color version of this figure is available in the online journal.)

our simulations we have kept terms up to $n = 2$ such that α_1 and α_2 are non-zero.

The second non-Gaussian model has the input PDF of the temperature field as an even power of a Gaussian PDF (Gaussian power model), with the temperature fluctuation value of the kth pixel given by

$$f(k) = g^{2p}(k),$$

where g is a zero mean, unit variance Gaussian variable, and p is chosen to be a positive integer. We have used $p = 1$ for our simulations.

Figure 6 shows the non-Gaussian deviations of n_h and n_c for these two models. Δn_i is again defined as given in Equation (6). The left panel shows the deviations for the SHO model and the right panel shows those for the Gaussian power model. As in the

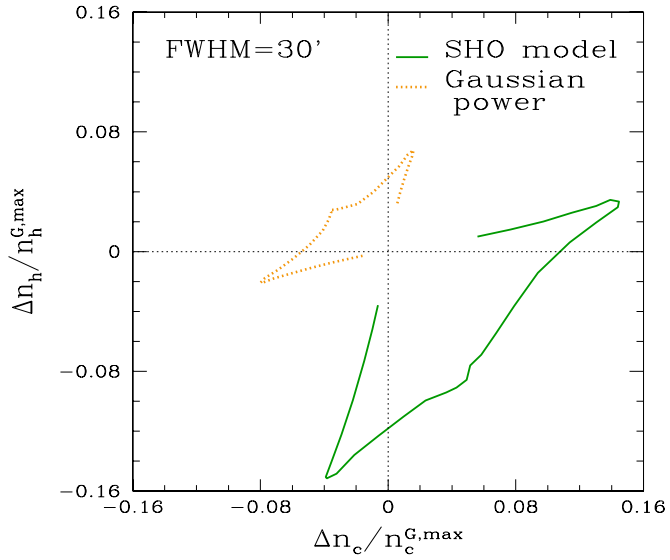

Figure 7. Plots of Δn_h vs. Δn_c for SHO (green, solid line) and Gaussian power (brown, dotted line) models.

(A color version of this figure is available in the online journal.)

local non-Gaussianity case we can see characteristic deviations for each type of non-Gaussianity.

For these models they do not have any simple correlation between Δn_h and Δn_c such as what we have seen for the local type non-Gaussianity, indicating that they carry information independent from each other. Figure 7 shows Δn_h versus Δn_c at each value of ν for these two models. These plots are a different way to characterize the type of non-Gaussianity of the HEALPIX non-Gaussian models.

4. STATISTICAL SENSITIVITY OF THE NUMBERS OF HOT AND COLD SPOTS TO $f_{\rm NL}$ AND $g_{\rm NL}$

To analyze the statistical power of n_h and n_c in realistic situations we measure them from simulations to which observational effects have been added. The observational effects are pixel window function, beam profile for each differential assembly (DA), and Gaussian noise realizations for each DA that follow the noise pattern, followed by Galaxy and point source masking. We then co-add Q, V, and W DA's with appropriate weights obtained from the inverse of the full-sky-averaged pixel-noise variance in each DA, and then smooth the field. For Galaxy masking we use the KQ75 mask. In Figure 8 we have shown the sample variance error bars obtained from the 200 $Q + V + W$ co-added maps prepared as described above. It is immediately noticeable that the error bars for $g_{\rm NL}$ is larger than those of $f_{\rm NL}$ at each corresponding smoothing angle. This can be understood from Equation (4) as follows. Suppose we have a perfectly Gaussian field ϕ^G and another "Gaussian" field with slight statistical fluctuations $\phi' = \phi^G(1 + D)$, where D quantifies the fluctuation. Then the deviation from the Gaussian field when $f_{\rm NL}$ and $g_{\rm NL}$ contributions are present is given by $\Delta\phi^{\rm NG} = D\phi^G + 2D\, f_{\rm NL}(\phi^G)^2 + 3D\, g_{\rm NL}(\phi^G)^3$. Hence statistical fluctuations seen for $g_{\rm NL}$ will be larger than those for $f_{\rm NL}$.

As a simple way of estimating the statistical discriminating power of the numbers of hot and cold spots in comparison to the genus we integrate the absolute values of the non-Gaussian

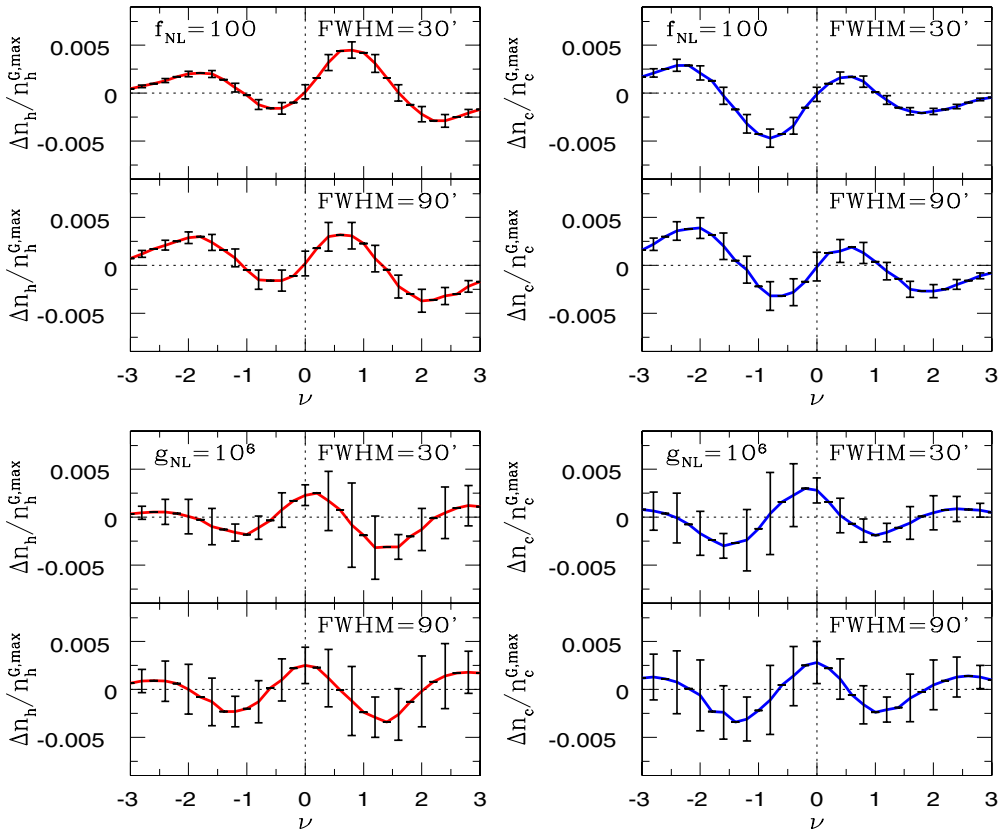

Figure 8. Non-Gaussian deviations of n_h and n_c for $f_{\rm NL}$ (upper panels) and $g_{\rm NL}$ (lower panels) calculated after adding observational effects, namely, pixel window function, beam profiles, noise for each DA, and galaxy and point source masking, to the simulations. These calculations are from $Q + V + W$ co-added maps. The error bars are the sample variance from 200 simulations.

(A color version of this figure is available in the online journal.)

Table 1
Values of A Defined in Equation (9) for g, n_h, and n_c

Non-Gaussian Input	Smoothing FWHM	Observable	A
$f_{\rm NL} = 100$	$30'$	g	7.4
		n_h	11.3
		n_c	11.3
	$90'$	g	3.3
		n_h	7.3
		n_c	7.5
$g_{\rm NL} = 10^6$	$30'$	g	2.0
		n_h	2.5
		n_c	2.5
	$90'$	g	1.1
		n_h	2.2
		n_c	2.1

deviations measured in units of the corresponding sample variances from $\nu = -3$ to 3. Let us denote it by A. For M threshold levels with spacing $\Delta\nu$, we can calculate it as

$$A = \Delta\nu \sum_{i=1}^{M} (|\Delta O(i)|/O^{G,\max})/\sigma_s(i), \quad (9)$$

where O can be either g, n_h, or n_c, and $\sigma_s(i)$ are the respective sample variances at each threshold level i. For our case, $M = 31$ and $\Delta\nu = 0.2$. The resulting values are shown in Table 1. We find considerably larger values of A for n_h and n_c compared to g both for $f_{\rm NL}$ and $g_{\rm NL}$ type non-Gaussianities, at the smoothing angles we have considered. This demonstrates that there is loss of statistical power for detecting the presence of non-Gaussian deviations when we combine n_h and n_c to get the genus.

5. CONCLUSION

We have introduced the numbers of hot and cold spots of the CMB temperature fluctuation field as statistical observables in their own right and propose to use them as discriminants of non-Gaussianity. We have studied the theoretical predictions for the numbers of hot and cold spots and their expected non-Gaussian deviations for various kinds of non-Gaussianities. We have calculated them using numerical methods from simulated CMB maps containing the different non-Gaussian models as inputs. The first type of input non-Gaussian model we studied is the so-called local type primordial non-Gaussianity, parameterized by $f_{\rm NL}$ and $g_{\rm NL}$ at the first and second order nonlinearities, respectively, of the perturbative expansion of the primordial gravitational potential. This gravitational potential is convolved with the full radiation transfer kept to linear order to obtain the simulated CMB temperature field, and hence the non-Gaussian deviations seen in the numbers of hot and cold spots are direct probes of the primordial non-Gaussianity. For these local primordial non-Gaussian models, what we find is that n_h and n_c are correlated as given by Equation (7). The strengths of the non-Gaussian deviations of n_h, n_c, and g are large at different regions of ν and hence each of them best probe regions of the field values specific to it. Therefore, they provide complementary information. Further, we have demonstrated that there exists additional information in the numbers of hot and cold spots compared to their linear combination given by the genus.

The second class of non-Gaussian models that we have considered assumes specific forms of the PDF of the temperature fluctuation field. In particular, we studied a model where the simulated temperature value at each pixel is drawn from a PDF given as an expansion in SHO states. We also studied another model where the temperature fluctuation values at each pixel is given as even powers of a number drawn from a Gaussian distributed field. Note that the assumption of the form of the PDF does not tell us anything about the physical source of the non-Gaussianity. Even though the physical origin of the non-Gaussianity is not clear, they are quite interesting models because they provide examples of non-Gaussian models where n_h and n_c are not correlated.

It is interesting to compare the shapes of the numbers of hot and cold spots with those of maxima and minima counts (Pogosyan et al. 2011; Bardeen et al. 1986; Bond & Efstathiou 1987; Adler 1981). The shapes of n_h and n_c are roughly similar to the maxima and minima counts, respectively, though the precise shape information such as peak location and the amplitude is quite different. Note that the extrema counts will measure more number of objects per unit area in comparison to the numbers of hot and cold spots since a typical connected/hole region can have more than one maxima/minima. As $|\nu|$ becomes much larger than one, n_h and n_c should tend toward the maxima and minima counts, respectively.

Our next goal is to apply the number of hot and cold spots to observational data and constrain $f_{\rm NL}$ and $g_{\rm NL}$. It would also be very useful to have their analytic expressions. We are presently working toward these directions.

We thank the Korea Institute for Advanced Study for providing computing resources (KIAS Center for Advanced Computation Linux Cluster System QUEST) where the local non-Gaussian simulations used in this paper were computed. We also acknowledge use of the Hydra cluster at the Indian Institute of Astrophysics for a part of the analysis. We acknowledge use of the HEALPIX package.

REFERENCES

Adler, R. J. (ed.) 1981, The Geometry of Random Fields (London: John Wiley & Sons)
Bardeen, J. M., Bond, J. R., Kaiser, N., & Szalay, A. S. 1986, ApJ, 304, 15
Bond, J. R., & Efstathiou, G. 1987, MNRAS, 226, 655
Chingangbam, P., & Park, C. 2009, J. Cosmol. Astropart. Phys., JCAP12(2009)019
Coles, P. 1988, MNRAS, 234, 509
Coles, P., & Barrow, J. D. 1987, MNRAS, 228, 407
Curto, A., Martínez-González, E., Barreiro, R. B., & Hobson, M. P. 2011, MNRAS, 417, 488
Gay, C., Pichon, C., & Pogosyan, D. 2012, Phys. Rev. D, 85, 023011
Górski, K. M., Hivon, E., Banday, A. J., et al. 2005, ApJ, 622, 759
Gott, J. R., III, Park, C., Juszkiewicz, R., et al. 1990, ApJ, 352, 1
Hikage, C., Komatsu, E., & Matsubara, T. 2006, ApJ, 653, 11
Hikage, C., Matsubara, T., Coles, P., et al. 2008, MNRAS, 389, 1439
Komatsu, E., Dunkley, J., Nolta, M. R., et al. 2009, ApJS, 180, 330
Komatsu, E., Smith, K. M., Dunkley, J., et al. 2011, ApJS, 192, 18
Liguori, M., Matarrese, S., & Moscardini, L. 2003, ApJ, 597, 57
Matsubara, T. 2003, ApJ, 584, 1
Matsubara, T. 2010, Phys. Rev. D, 81, 083505
Pogosyan, D., Gay, C., & Pichon, C. 2009, Phys. Rev. D, 80, 081301
Pogosyan, D., Pichon, C., & Gay, C. 2011, Phys. Rev. D, 84, 083510
Rocha, G., Hobson, M. P., Smith, S., Ferreira, P., & Challinor, A. 2005, MNRAS, 357, 1
Schmalzing, J., & Gorski, K. M. 1998, MNRAS, 297, 355
Seljak, U., & Zaldarriaga, M. 1996, ApJ, 469, 437
Smidt, J., Amblard, A., Byrnes, C. T., et al. 2010, Phys. Rev. D, 81, 123007
Tomita, H. 1986, Prog. Theor. Phys., 76, 952
Vanmarcke, E. (ed.) 1983, Random Fields: Analysis and Synthesis (Cambridge, MA: MIT Press)
Vielva, P., & Sanz, J. L. 2010, MNRAS, 404, 895
Winitzki, S., & Kosowsky, A. 1998, New Astron., 3, 75